Available online at www.sciencedirect.com
ScienceDirect
Journal of the European Ceramic Society 29 (2009) 1337–1345
www.elsevier.com/locate/jeurceramsoc

Synthesis and two-step sintering behavior of sol–gel derived nanocrystalline corundum abrasives

Zicheng Li, Zhihong Li *, Aiju Zhang, Yumei Zhu

Key Laboratory of Advanced Ceramics and Machining Technology, Ministry of Education, School of Materials Science and Engineering, Tianjin University, Tianjin 300072, PR China

Received 29 June 2008; received in revised form 29 August 2008; accepted 11 September 2008
Available online 13 January 2009

Abstract

Nanocrystalline corundum abrasive with mean crystal size of less than 100 nm was synthesized by two-step sintering method using sol–gel process. A remarkable suppression of grain growth was achieved by controlling sintering temperature and taking advantage of sintering aids during the final stage of a two-step sintering process. The grain size of the high densification samples (>99% theoretical density) produced by two-step sintering method was about 10 times less than the samples made by the conventional sintering technique. The microstructure of the samples was homogeneous without abnormal grain growth and the sol–gel derived corundum abrasive with two-step sintering technique exhibited excellent mechanical properties and wear resistance compared to those sol–gel derived corundum abrasive with conventional sintering methods and fused corundum abrasive.

Keywords: Sintering; Sol–gel processes; Grain size; Al_2O_3; Wear parts

1. Introduction

Recent interests in synthesis and sintering of microcrystalline corundum abrasives have grown due to the significant improvement in their properties, especially high hardness, high strength, good wear resistance and long service life, as compared to the conventional coarser single crystalline fused-corundum abrasives.[1–5] Synthesis of microcrystalline corundum abrasives by traditional pressureless sintering technique has been reported during the past decades.[6–10] The primary goal for obtaining microcrystalline corundum abrasives are full densification and grain-size control.[11] In addition, uniformity of the microstructure should be taken into account as another key factor when one considered that the wearability is a sensitive function of the grain sizes. Unfortunately, corundum abrasives using pressureless sintering method with grain size less than 100 nm have not been reported. Sintering is the process whereby interparticle pores in a granular material are eliminated by atomic diffusion driven by capillary forces. But, these final-stage sintering processes are always accompanied by rapid grain growth,[12–15] because the capillary driving forces for sintering and grain growth (involving grain boundaries) are comparable in magnitude, both being proportional to the reciprocal grain size. This has greatly hampered efforts to produce dense corundum composites with nanometre-scale structure,[16] leading many researchers to resort to the high-cost approach of high-pressure consolidation at elevated temperatures.[17,18] To fabricate fine crystalline corundum abrasives by pressureless sintering route, grain boundary migration has to be abated. The grain growth can be controlled by two approaches: one is to prohibit grain growth by addition or dispersion of a second phase particles[19–23]; the other is to control grain growth by a novel processing method. It was first reported that a two-step sintering (TSS) technique can be also used as an efficient route to attain a homogeneous microstructure and to decrease the number of closed pores.[24] In TSS technique the sample was first heated to a higher temperature then cooled down to a lower temperature to suppress grain-boundary migration, and held at that temperature till full densification. Such a TSS method is effective to obtain nanoceramics such as Y_2O_3 and Si_3N_4 nanoceramics.[25,26] However, fabrication of corundum abrasives by TSS technique has not been reported.

The main objective of this study was to obtain high dense corundum abrasive with a grain size less than 100 nm by a sim-

* Corresponding author. Tel.: +86 22 2740 4260; fax: +86 22 2740 4260.
E-mail address: lizhihong@tju.edu.cn (Z. Li).

0955-2219/$ – see front matter © 2009 Elsevier Ltd. All rights reserved.
doi:10.1016/j.jeurceramsoc.2008.09.004

ple two-step sintering process, at temperature of about 1300 °C without applied pressure. The suppression of the second-stage grain growth was investigated by exploiting the difference in kinetics between grain-boundary diffusion and grain-boundary migration. The sintering behavior and microstructural evolution during densification of normal and TSS process are compared. The effect of microstructure on the mechanical properties has also been discussed.

2. Experimental procedures

2.1. Materials and synthesis

The hydrous alumina was prepared by adding $NH_3{\cdot}H_2O$ solution (0.2 mol l^{-1}) slowly to a rapidly stirred commercial $Al_2(SO_4)_3{\cdot}18H_2O$ ($Al_2O_3 > 16$ wt.%, Zbdazhong Ltd., Zibo, China) solution (0.3 mol l^{-1}). PEG (molecular weight 1000) solution was used as dispersant to prevent the powder from agglomerating. The sol pH was adjusted to 9.7, and then stirred in magnetic stirring apparatus at 60 °C for 2 h. After separation from the mother solution by filtration, the resulting precipitate was washed three times with water to remove SO_4^{2-} ion. The washed precipitate was milled with water by adding α-Al_2O_3 seed (grain size < 0.2 μm) and sintering additives (MgO, CaO and SiO_2) for 10 h in a polyethylene jar. The sintering additives were introduced in the form of magnesium nitrate $Mg(NO_3)_2{\cdot}6H_2O$ (AnalaR grade, Kewei Ltd., Tianjin, China), calcium nitrate $Ca(NO_3)_2{\cdot}4H_2O$ (AnalaR grade, Kewei Ltd., Tianjin, China) and tetraethylorthosilicate (TEOS) (AnalaR grade, Kewei Ltd., Tianjin, China). The amount of sintering additive components was adjusted to be equivalent to 2.5 wt.% with MgO:CaO:SiO_2 molar ratio 5:1:5 (composition which is near to the eutectic point in the MgO–CaO–SiO_2 ternary phase diagram). Then the solid residue was dried for 24 h at 80 °C and crushed to obtain the xerogel particles.

In order to compare with sol–gel derived corundum abrasive, commercial fused corundum abrasive (Ruishi Special Refractory Ltd., Henan, China) (fused sintering, named as FS) was also used as raw materials.

2.2. Sintering

The xerogel particles were sintered at 1150–1300 °C used two steps in the heating schedule. At first step, samples were heated up to the higher temperature (named hereafter as T_1) without holding time. They were then cooled down to the lower temperature (named hereafter as T_2) and held at T_2 for 5 h. In order to establish the TSS conditions, single-step sintering runs (conventional sintering, named as CS) were conducted at temperature T_1. In the single-step sintering runs at temperature T_1, the samples were heated to T_1 and held at T_1 for 5 h, then cooled down to room temperature. In order to compare with TSS method, the third sintering method (named as CTS) was also employed. That is, the samples were heated to T_1 without holding time and cooled down to room temperature, then these sintered samples were heated at temperature T_2 and held at T_2 for 5 h. These sintered techniques were listed in Table 1.

The density of the sintered samples was measured according to Archimedes method in deionized water and the average value was reported. The θ-Al_2O_3 to α-Al_2O_3 phase transformation of the xerogel was examined by thermogravimetry–differential scanning calorimetry (TG-DSC, NETZSCH STA 449C, Germany) heating 15 mg samples in Pt cups at a rate of 10 °C min^{-1} using ignited alumina as the reference material. The particle phase was identified using an X-ray diffractometer (XRD, PHILIPS X'Pert-MPD System) with Ni-filtered Cu Kα radiation. Microstructure of the sintered products was analyzed by field emission scanning electron microscopy (FESEM, JEOL JSM-6700F, Japan). Quantitative chemical analyses were performed using energy dispersive X-ray spectrometry (EDS) at 25 keV. The grain size was determined from the micrographs using the linear intercept method from SEM micrographs[27]:

$$\overline{D} = 1.56\frac{C}{MN} \quad (1)$$

where $\overline{D}$ is the average grain size of the corundum abrasive samples used in the experiment, C the measuring line length, M the magnification times of samples and N the number of the sections in the micrograph.

Table 1
Characterization of tested corundum abrasives.

Sintered condition	Designation of sintered sample	Temperature/°C	Relative density/%	Average grain size/nm	Hardness/GPa	Fracture toughness/MPa $m^{1/2}$
CS						
T_1-5 h	CS_1	1250	92.1	680	19.13 ± 0.34	2.86 ± 0.08
	CS_2	1300	93.4	800	19.55 ± 0.43	2.75 ± 0.17
CTS						
(T_1-0 h) + 25* + (T_2-5 h)	CTS_1	1250-25-1150	96.0	400	20.31 ± 0.19	2.93 ± 0.09
	CTS_2	1300-25-1150	97.5	560	20.82 ± 0.22	2.91 ± 0.12
TSS						
(T_1-0 h) + (T_2-5 h)	TSS_1	1250-1150	99.1	65	22.39 ± 0.17	3.37 ± 0.06
	TSS_2	1300-1150	99.6	80	22.54 ± 0.21	3.21 ± 0.11
Fused corundum**	FS	–	99.5	–	20.60 ± 0.32	2.23 ± 0.14

* 25 °C was the room temperature in Section 2.
** Commercial fused corundum abrasive with single crystalline grains, the hardness and its fracture toughness were determined.

2.3. Mechanical properties and wear test

Compacts were sintered at various sintering temperatures. After classification with screen of 60/80 mesh, these sintered abrasive particles (particle size in the range of 0.2–0.3 mm) were measured by using a single particle compressive strength tester (ZMC-II, China). One particle was tested every time. An average of 40 particles per sample were reported.

In order to measure the wear resistance of corundum abrasives, simple grinding wheel (diameter 50 mm and width 12 mm) was prepared using a vitrified bond (matured at 900 °C) and corundum abrasive particles. All the wear tests were carried in normal laboratory air at ambient temperature between 20 and 25 °C, and the relative humidity around 35%. Simple grinding wheel unidirectional wear and friction testing machine was used for this study. Each sample was ultrasonically cleaned and dried before and after the experiment. Volumetric wear of grinding wheel was calculated from gravimetric measurement. All the experiments were conducted under the following conditions: 25 cm diameter metal bonded 120-grit diamond wheel with a sliding speed of 0.2 m/s under a constant rotational speed of 50 rpm. Each test was continued up to a sliding distance of 7.2 km with the normal load of 50 N. The samples were weighed before and after the test on an electronic microbalance (METTLER TOLEDO, PL-203, Germany). Each experiment was repeated at least thrice to check the reproducibility of data. The wear rate of the worn out samples were calculated by using the following equation:

$$W_R = \frac{\Delta V}{FS} \tag{2}$$

where W_R is the wear rate of samples, ΔV the volume loss due to wear, F the normal load and S the sliding distance.

Hardness and fracture toughness assessments of samples were carried out using the indentation method. After wear rate measurements, disks were cut using a diamond wheel and polished by diamond paste to 1 μm finish. Polished abrasive particles were used for Vickers indentation testing. Indentation test was conducted with a load of 10 N and an impression time of 20 s. The Vickers hardness (H_V) was calculated from the diagonal length of the indentation determined by SEM observation according to the following equation[28]:

$$H_V = 1.854\frac{P}{d^2} \tag{3}$$

where P is the load and d is the average value of the diagonal length. Fracture toughness (K_{IC}) was determined according to the following equation[29]:

$$K_{IC} = 0.016\left(\frac{E}{H_V}\right)^{1/2}\left(\frac{P}{C^{3/2}}\right) \tag{4}$$

where E is the Young's modulus, H_V the Vickers hardness and C is half the crack diagonal. For each result at least five indentations were carried out and the mean values are reported.

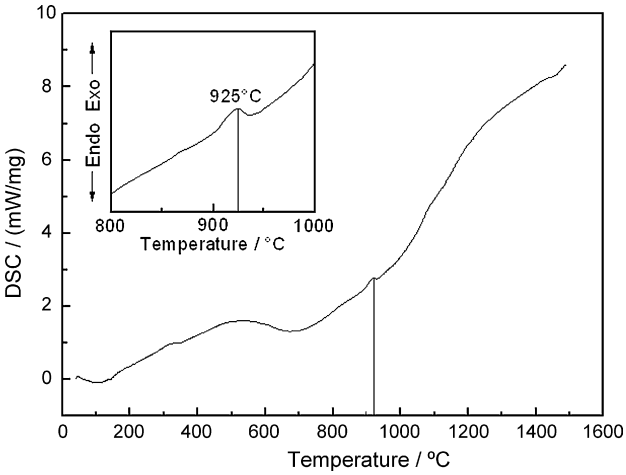

Fig. 1. Thermal behavior of the milled xerogel with seeding and additives (heating rate 10 °C min^{-1}).

3. Results and discussion

3.1. Phase transformations of the xerogel upon heating

Thermal behavior of the milled xerogel with seeding and additives was shown in Fig. 1, which was determined by DSC up to 1500 °C at a heating rate of 10 °C min^{-1}. From DSC curve it can be seen that the endothermic peak existed at about 200 °C due to evaporation of absorbed water. The exothermic peak (at about 600 °C) was assigned to the PEG burnout and the 925-°C peak is associated with the phase transformation and crystallization of α-Al_2O_3, which was in agreement with the XRD results in Fig. 2.

The dried gel with seeding and additives calcined at 800, 900, 925 and 1000 °C, respectively were identified by XRD, as shown in Fig. 2. The dried gel sample calcined at 900 °C can be partly converted to α-Al_2O_3, but the characteristic peak of θ-Al_2O_3 existed at 900 °C with low intensity. The degree of crystallinity

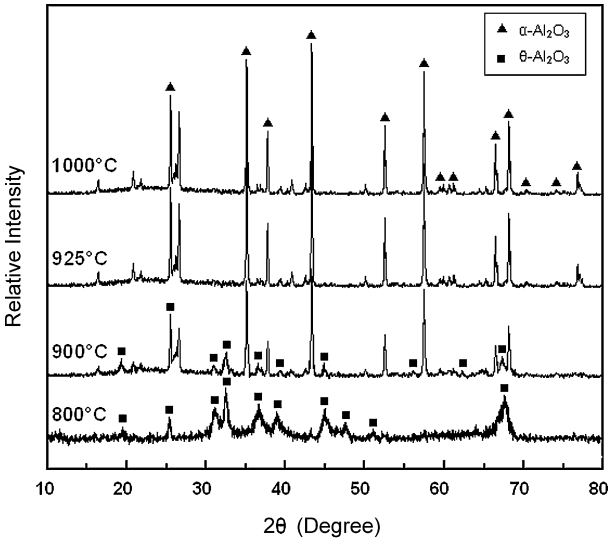

Fig. 2. XRD patterns of the samples sintered at 800, 925, 950 and 1000 °C.

of α-Al_2O_3 was improved with increasing temperature. θ-Al_2O_3 was completely transformed to α-Al_2O_3 at 925 °C. Therefore, when 1250 °C were employed in TSS process, it was sure that θ-Al_2O_3 was completely transformed to α-Al_2O_3.

3.2. Microstructure and densification characterization

The density and the average grain size of the sintered corundum abrasive as a function of the peak temperature were shown

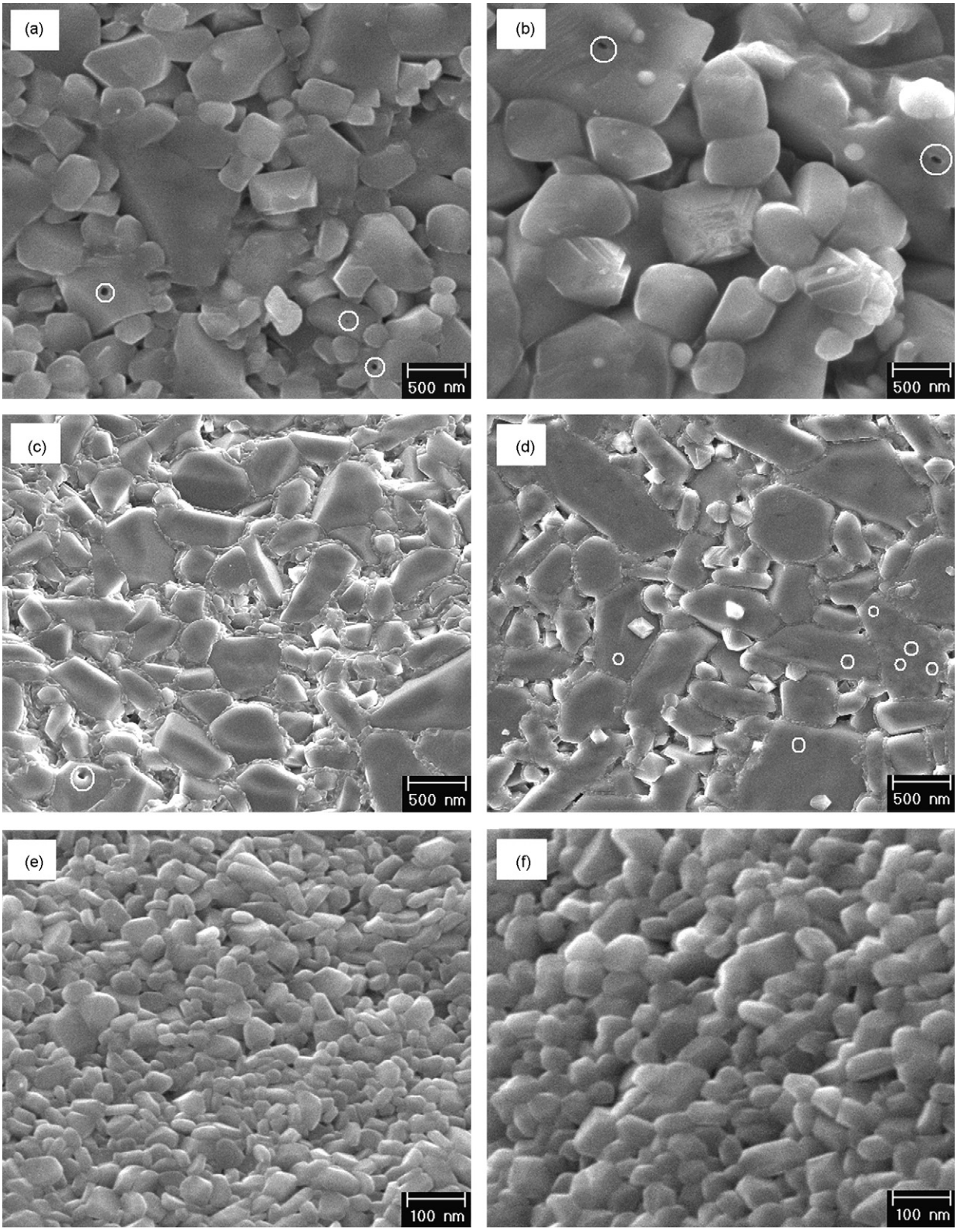

Fig. 3. Micrographs of corundum abrasive samples sintered by different processes: (a) CS_1; (b) CS_2; (c) CTS_1; (d) CTS_2; (e) TSS_1 and (f) TSS_2.

in Table 1. In the CS method at temperature of T_1 for 5 h, the maximal densities of the samples reached 92.1–93.4%TD corresponding to the peak temperature of 1250–1300 °C. In the CTS method at temperature of T_2, the density of samples varied between 96.0 and 97.5%TD. In the TSS process, the product densities of above 99.1%TD were generally achieved. The average grain size was various with the different sintering techniques, the corresponding average grain size of the samples CS_1, CS_2, CTS_1, CTS_2, TSS_1 and TSS_2 were 680, 800, 400, 560, 65 and 80 nm. And in the TSS method, the average grain size of samples was less than 100 nm.

Fig. 3 shows the SEM microstructures of corundum abrasive samples sintered by different processes. From the microstructures, coarse grains larger than 500 nm could be observed in the samples sintered with CS and CTS method (Fig. 3(a)–(d)). Note that the grains with abnormal grain growth were existed and many pores were located both on grain boundaries and within the grains (see circled regions). While in the TSS process, the microstructure with fine crystalline of the TSS_1 and TSS_2 samples (Fig. 3(e) and (f)) remained homogeneous without abnormal grain growth. Fig. 4 demonstrated that average grain size distribution of near full dense samples sintered by CTS and TSS methods, in which average grain size distribution of CTS_2 and TSS_2 samples were evaluated based on the observations from SEM micrographs of their full dense specimens. The narrower distribution of the grain size in the TSS_2 sample could be described by the higher microstructural homogeneity resulted from TSS in comparison with CTS.

In Fig. 5, after a starting average grain size was obtained during the first step, with increasing holding time (from 0 to 5 h), full densification without grain growth was achieved with the TSS method. Note that the average grain size remained constant in the second sintering step, despite density improvement to near 100%. These results were entirely different from those of CS and CTS processes. Even with fine starting grain (The grain sizes of CS_1, CS_2, CTS_1 and CTS_2 were less than 100 nm with the holding time for 0 h), the final grain size of dense samples was well over 400 nm after holding time for 5 h. Therefore, it was evident

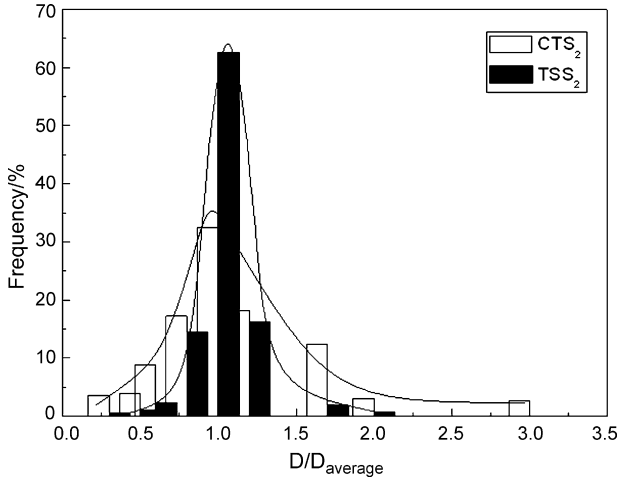

Fig. 4. The grain size distribution of near full dense samples sintered by CTS and TSS methods.

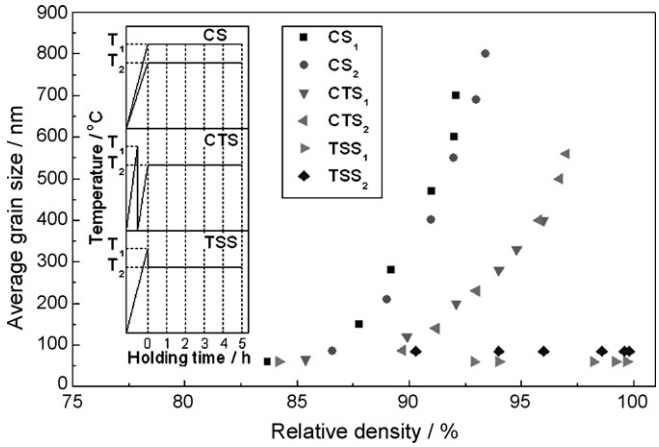

Fig. 5. Average grain size of samples with density in CS, CTS and TSS methods. (Heating schedule shown in inset.).

that when the two steps were conducted in succession, the second step sintering was effective to promote further densification without grain growth. It was because a sufficiently high starting density was obtained at temperature of T_1, all pores in samples became subcritical and unstable against shrinkage. Continuous microstructural framework formed among crystallines and acted as atom diffusion path driving the subsequent sintering step. The activation for the grain boundary diffusion was far lower than that for the grain boundary migration. The energy obtained at the first step was sufficient for the grain boundary diffusion in the holding process during the second step sintering at temperature of T_2. Promoted by grain boundary controlled kinetics, near full densification of the samples, especially without grain growth, was achieved.

Furthermore, the influence of MgO–CaO–SiO_2 as sintering aid on the properties of the samples was taken into account. Because they as the silicate had a marked grain-boundary-strengthening action and as grain-boundary phase could clearly suppressed grain-growth when the grain zone were completely covered by the continuous silicate phase, even at extremely low concentrations.[30] The calcium silicate-densified alumina examined earlier showed the amorphous silicate films at all the two-grain boundaries, of order of 2 nm thickness.[31] The SEM examinations (Fig. 7(a)) of the magnesium calcium silicate-densified corundum materials used here also showed continuous film of amorphous silicate at both grain-boundary and grain surface in the sample sintered by TSS method. While in the sample sintered by CTS processing (Fig. 6(a)), the crystalline secondary phases were observed in the grain boundaries. It was suggested that continuous film of amorphous silicate at both grain-boundary and grain surface was broken. This was because that Si, Ca and Mg ions diffused to the boundary and the amorphous phase was transformed into crystalline state in the grain boundary. For this reason, the grain boundary mobility of alumina was not hindered in the grain zone. Consequently, the grain growth was occurred. This observation was supplemented by EDS microanalysis. EDS microanalysis done on the different areas of grain and grain-boundary showed the composition of both CTS_2 and TSS_2, as illustrated

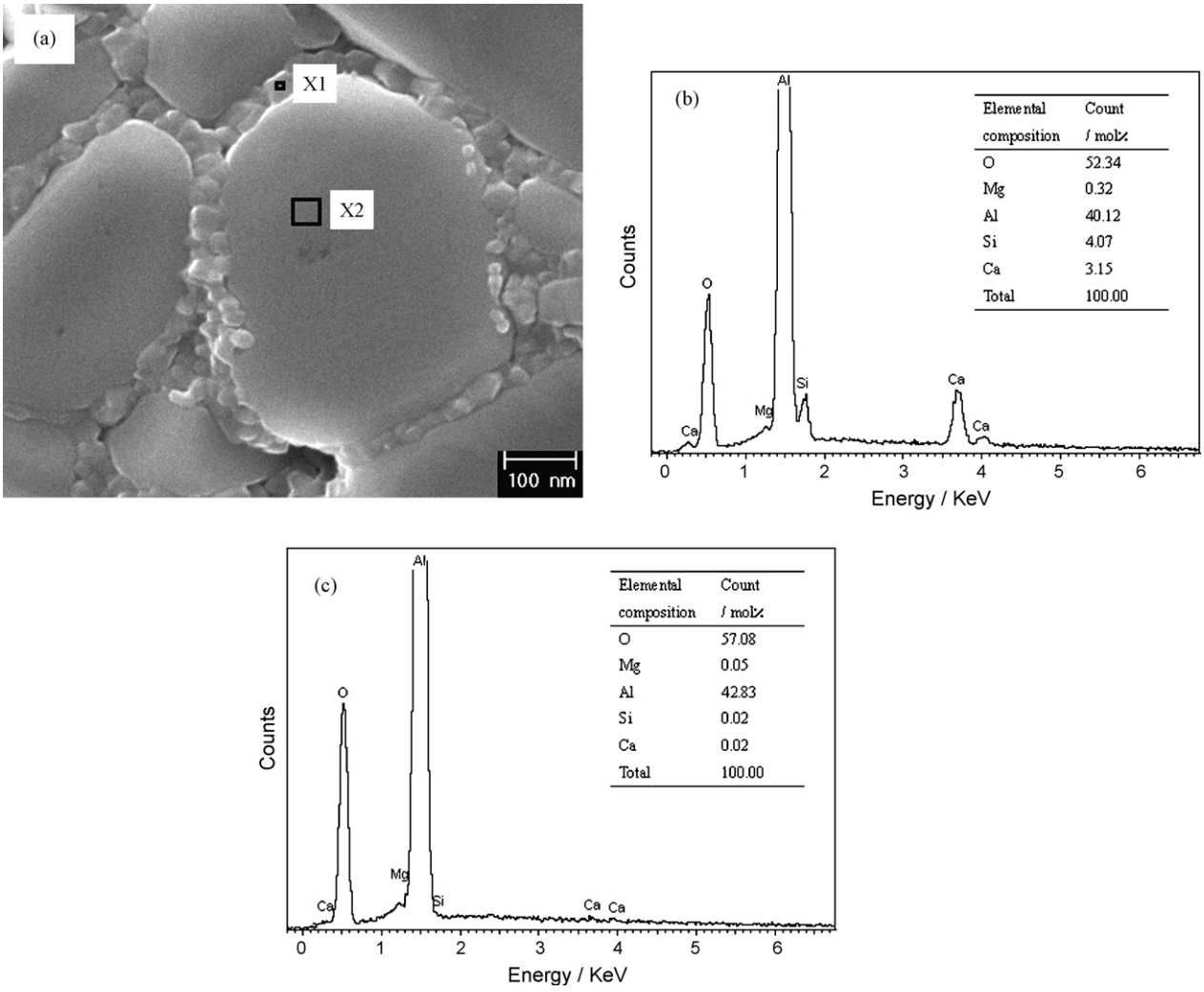

Fig. 6. (a) SEM image of sample sintered by CTS method and EDS spectrum of (b) mark X1 and (c) mark X2.

in Fig. 6(b) and (c), Fig. 7(b) and (c). For the TSS_2 sample, the grain surface and grain boundary had approximately equal proportions of Mg:Ca:Si (expressed as atomic percent). Whereas for the CTS_2 sample, the grain boundary regions (second-phase crystalline particle) were rich in silicon and calcium. The composition of Mg, Ca and Si was few in grain surface. It was indicated that the uniform distribution of these sintering aid was failed. This showed that grain-boundary migration was unsuppressed and grain growth occurred.

3.3. Mechanical property

The influence of sintering techniques on single particle compressive strength of abrasive particle samples was shown in Fig. 8. Fused corundum abrasive had a minimal compressive strength value (16.6 N). The samples sintered by CS method had much lower strength (less than 22.5 N) compared to that fabricated by CTS and TSS methods, which was due to low density and nonuniform microstructure with abnormal grain growth. For the samples sintered by CTS processing, the degradation of samples in compressive strength should be attributed to the formation of the secondary crystalline phases in the grain boundaries, which decreased the bond strength between grain and grain-boundary. While in the sample sintered by TSS processing, the grains were completely covered by continuous amorphous silicate films. The high compressive strength was undoubtedly attributed to high bond strength among grains, the high density and homogeneous structure with fine grain size. On the other hand, the mismatch of thermal expansion coefficient between amorphous silicate films and alumina grains, would be expected to lead to residual stresses after cooling to room temperature.[32,33] This mismatch stress most likely contributed to the promotion of compressive strength.

The microhardness and fracture toughness of the investigated samples are shown in Table 1. Interestingly, the hardness of fused corundum abrasive is 21.60 ± 0.32 Gpa, but the fused corundum abrasive had a lowest fracture toughness of $1.98 \pm 0.14\ \mathrm{MPa\,m^{1/2}}$ compared to samples with CS, CTS and TSS methods. It is observed that fracture toughness increases with decreasing the average grain size and reaches a maximum value of $3.37 \pm 0.06\ \mathrm{MPa\,m^{1/2}}$ for TSS_1 sample with average grain size of 65 nm. These data show the samples with fine crystalline microstructure via TSS technique had higher mechanical properties.

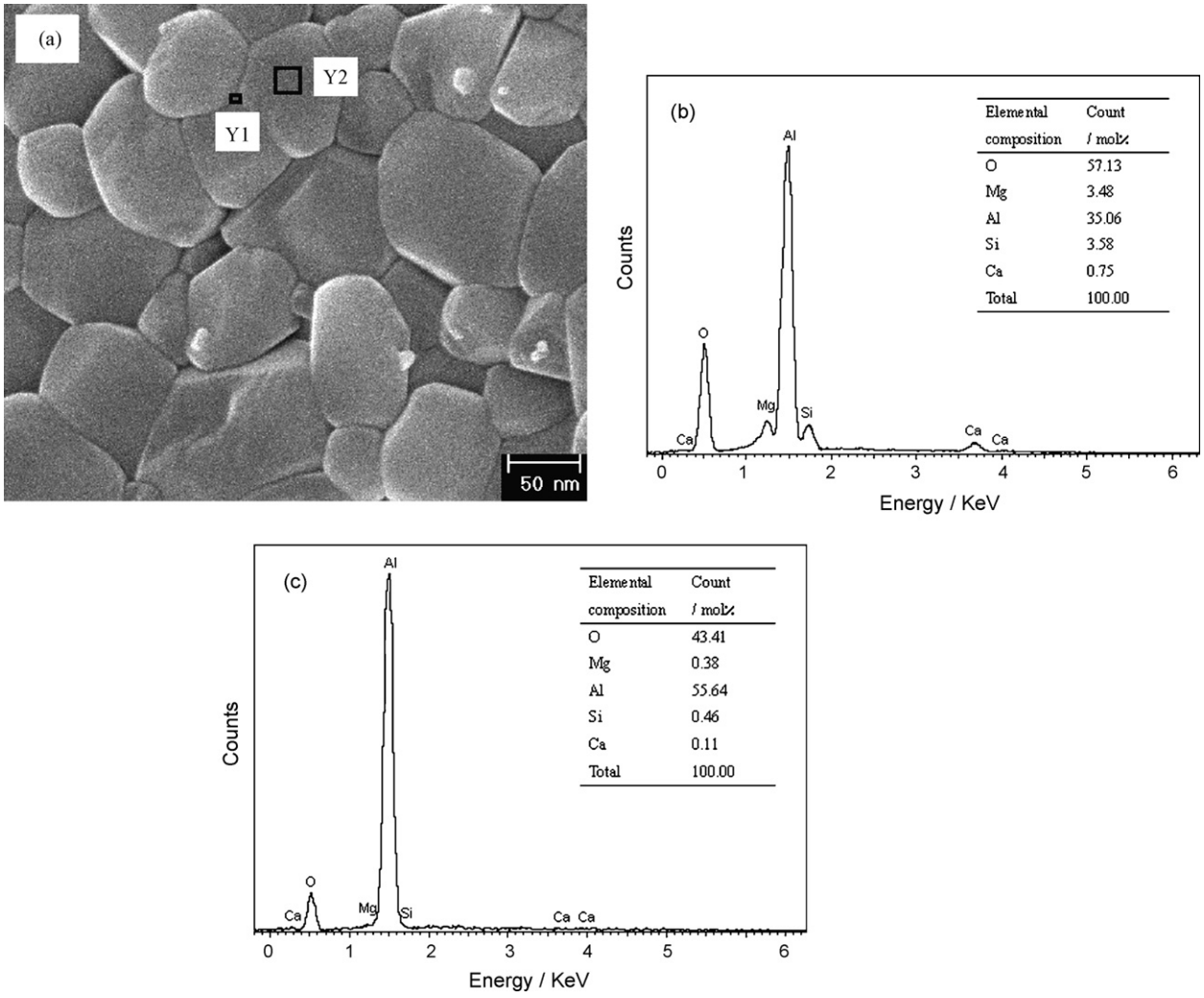

Fig. 7. (a) SEM image of sample sintered by TSS method and EDS spectrum of (b) mark Y1 and (c) mark Y2.

3.4. Wear behavior

Wear resistances of the grinding wheel samples sintered by CS, CTS and TSS methods were presented in Fig. 9. Wear resistances of the grinding wheel samples also, represented the similar trend like the influence of sintering technique variation on the single particle compressive. In Table 1, it was shown that the average grain size of samples sintered by CS was higher than that sintered by CTS and TSS, and the grain size of sample sintered by TSS was minimal. And from Fig. 9, it was suggested that a reduction in the value of the grain size resulted in a marked abradability increase in the sintered specimens. That is, if the grain size is smaller, the crack encounters triple junctions more frequently and the overall rate of crack propagation is lower.[34] Furthermore, in the wear process, as intergranular microfracture and crystal dislodgement occurred through microcrack propagation along individual crystal boundaries, crystal boundary toughness became guiding factor for wear loss in such situation. So the wear rate of samples sintered by TSS processing which had more compacted intergranular structure and greater crystal boundary toughness for its uniform, fine crystal structure were minimal.

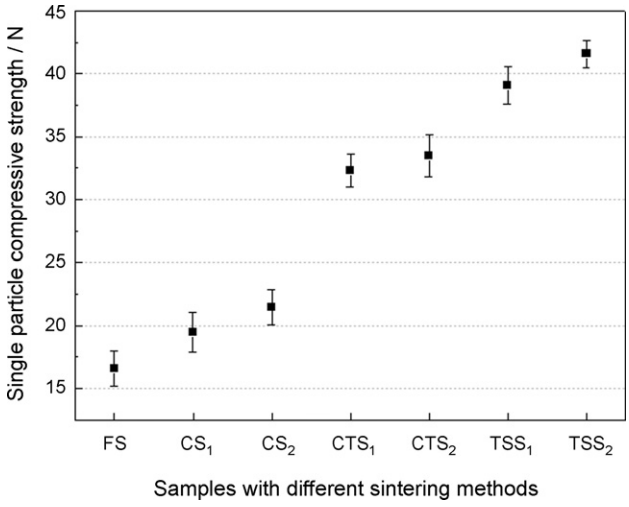

Fig. 8. The single particle compressive strength of abrasive particle samples sintered via FS, CS, CTS and TSS routes (particle size in the range of 0.2–0.3 mm).

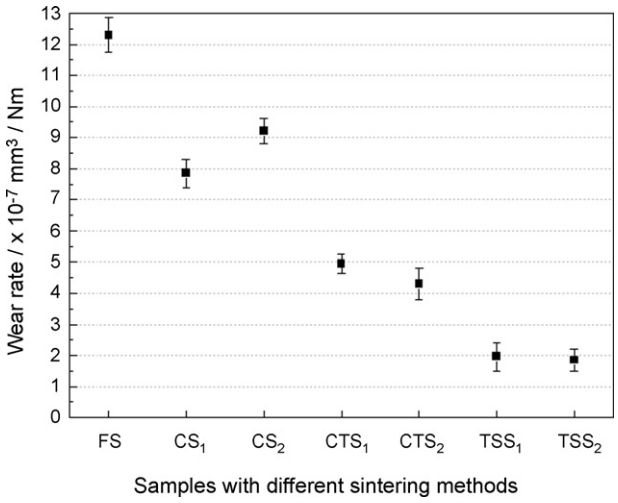

Fig. 9. The wear rate of samples sintered via FS, CS, CTS and TSS routes.

4. Conclusions

Nanocrystalline corundum abrasive was synthesized using sol–gel process. The microstructure evolution during CS, CTS and TSS methods was investigated. The single particle compressive strength and wear resistance of nearly full dense structures obtained by different sintering regimes were measured. The following results were obtained:

1. Two-step sintering significantly prohibited the grain growth in the final stage of sintering without deteriorating the densification process due to the grain-boundary diffusion. The value of final fractional density obtained by TSS procedure was above 99.1% TD. The TSS yielded the samples with a smaller grain size value (less than 100 nm), compared to CS (680–800 nm) and CTS (400–560 nm) methods.
2. $MgO–CaO–SiO_2$ not only served as an effective liquid phase sintering aid for surpressing grain growth and attaining near full densification, but also significantly promoted single particle compressive strength and wear resistance properties of corundum abrasives due to the formation of continuously amorphous silicate film.
3. The samples sintered by TSS method exhibited excellent single particle compressive strength (above 39.2 N) and wear resistance (less than $(1.86 \pm 0.45) \times 10^{-7}\,mm^3\,N^{-1}\,m^{-1}$) properties compared to FS, CS and CTS methods.

Acknowledgement

The authors would like to thank the Tianjin University of Technology for providing a research fellowship to FESEM.

References

1. Davidge, R. W., Twigg, P. C. and Riley, F. L., Effect of silicon carbide nanophase on the wet erosive wear of polycrystalline alumina. *J. Eur. Ceram. Soc.*, 1996, **16**, 799–802.
2. Anya, C. C., Wet erosive wear of alumina and its composites with SiC nano-particles. *Ceram. Int.*, 1998, **24**, 533–542.
3. Krell, A. and Blank, P., The influence of shaping method on the grain size dependence of strength. *J. Eur. Ceram. Soc.*, 1996, **16**, 1189–1200.
4. Roy, R. S., Guchhait, H., Chanda, A., Basu, D. and Mitra, M. K., Improved sliding wear-resistance of alumina with sub-micron grain size: a comparison with coarser grained material. *J. Eur. Ceram. Soc.*, 2007, **27**, 4737–4743.
5. Krell, A. and Blank, P., Advances in the grinding efficiency of sintered alumina abrasives. *J. Am. Ceram. Soc.*, 1996, **79**, 763–769.
6. Mayer, J., Engelhorn, R., Bot, R., Weirich, T., Herwartz, C. and Klocke, F., Wear characteristics of second-phase-reinforced sol–gel corundum abrasives. *Acta Mater.*, 2006, **54**, 3605–3615.
7. Cheng, J. P., Agrawal, D., Roy, R. and Jayan, P. S., Continuous microwave sintering of alumina abrasive grits. *J. Mater. Process. Technol.*, 2000, **108**, 26–29.
8. Herman, D., Plichta, J. and Karpiński, T., Effect of glass-crystalline and amorphous binder application to abrasive tools made of microcrystalline alumina grains type SG. *Wear*, 1997, **209**, 213–218.
9. Li, Z. C., Li, Z. H., Zhang, A. J. and Zhu, Y. M., Synthesis processes of nanoalumina abrasive. *Key Eng. Mater.*, 2008, 368–372, 619–693.
10. Bauer, R. and Skoweon, M. L., High temperature bonded abrasive for e.g. lapping application, has alumina abrasive grits distributed in vitreous bond matrix, where abrasive grits are provided with polycrystalline alpha alumina with fine crystalline microstructure. United States Patent 2,008,148,653-A1, December 12, 2007.
11. Cho, S. J., Hockey, B. J., Lawn, B. R. and Bennison, S. J., Grain-size and *R*-curve effects in the abrasive wear of alumina. *J. Am. Ceram. Soc.*, 1989, **72**, 1249–1252.
12. Cameron, C. P. and Raj, R., Grain growth transition during sintering of colloidally prepared alumina powder compacts. *J. Am. Ceram. Soc.*, 1988, **71**, 1031–1035.
13. Krell, A., Teresiak, A. and Schlafer, D., Grain size dependent residual microstresses in sub-micron Al_2O_3 and ZrO_2. *J. Eur. Ceram. Soc.*, 1996, **16**, 803–811.
14. Marshall, D. B., Lawn, B. R. and Cook, R. F., Microstructural effects on grinding of alumina and glass–ceramics. *J. Am. Ceram. Soc.*, 1987, **70**, 139–140.
15. Miranda-Martinez, Davidge, R. W. and Riley, F. L., Grain size effects on the wet erosive wear of high-purity polycrystalline alumina. *Wear*, 1994, **172**, 41–48.
16. Mayo, M. J., Processing of nanocrystalline ceramic from ultrafine particles. *Int. Mater. Rev.*, 1996, **41**, 85–115.
17. Gleiter, H., Nanocrystalline materials. *Prog. Mater. Sci.*, 1989, **33**, 223–315.
18. Liao, S. C., Chen, Y. J., Kear, B. H. and Mayo, W. E., High pressure/low temperature sintering of nanocrystalline alumina. *Nanostruct. Mater.*, 1998, **10**, 1063–1079.
19. Galusek, D., Kido, L., Pánek, Z., Lenčéš, Z., Šajgalík, P. and Riley, F. L., The influence of sintering additives on fracture behaviour and wear of liquid phase sintered polycrystalline alumina. *Key Eng. Mater.*, 2002, **223**, 227–232.
20. Giulio, R., Joseph, E. and Burke, Influence of additives on the microstructure of sintered Al_2O_3. *J. Am. Ceram. Soc.*, 1973, **56**, 654–659.
21. Song, H. and Coble, R. L., Origin and growth kinetics of platelike abnormal grains in liquid-phase-sintered alumina. *J. Am. Ceram. Soc.*, 1990, **73**, 2077–2085.
22. Xue, L. A. and Chen, I. W., Low-temperature sintering of alumina with liquid-forming additives. *J. Am. Ceram. Soc.*, 1991, **74**, 2011–2013.
23. Luo, J. and Stevens, R., The role of residual stresses on the mechanical properties of Al_2O_3–5 vol.% SiC nanocomposites. *J. Eur. Ceram. Soc.*, 1997, **17**, 1565–1572.
24. Kim, D. S., Lee, J. H., Sung, R. J., Kim, S. W., Kim, H. S. and Park, J. S., Improvement of translucency in Al_2O_3 ceramics by two-step sintering technique. *J. Eur. Ceram. Soc.*, 2007, **27**, 3629–3632.
25. Chen, I. W. and Wang, X. H., Sintering dense nanocrystalline ceramics without final-stage grain growth. *Nature*, 2000, **404**, 167–171.
26. Kim, H. D., Park, Y. J., Han, B. D., Park, M. W., Bae, W. T., Kim, Y. W. *et al.*, Fabrication of dense bulk nano-Si_3N_4 ceramics without secondary crystalline phase. *Scripta Mater.*, 2006, **54**, 615–619.

27. Mendelson, M. I., Average grain size in polycrystalline ceramics. *J. Am. Ceram. Soc.*, 1969, **52**, 443–446.
28. ASTM C1327-96, Standard test method for Vickers indentation hardness of advanced ceramics. *Annual Book of ASTM Standards*, vol. 15.01, 2003.
29. Anstis, G. R., Chantikul, P., Lawn, B. R. and Marshall, D. B., Acriticalevaluation of indentation techniques for measuring fracture toughness. 1 Direct crack measurements. *J. Am. Ceram. Soc.*, 1981, **64**, 533–538.
30. Galusek, D., Brydson, R., Twigg, P. C. and Riley, F. L., Wet erosive wear of alumina densified with magnesium silicate additions. *J. Am. Ceram. Soc.*, 2001, **84**, 1767–1776.
31. Brydson, R., Twigg, P. C., Chen, S. C., Riley, F. L. and Rühle, X. P., Migrostructure and chemistry of intergranular glassy films in liquid-phase-sintered alumina. *J. Am. Ceram. Soc.*, 1998, **81**, 369–379.
32. Powell-Dogan, C. A. and Heuer, A. H., Microstructure of a 96% alumina ceramic. II Crystallization of high-magnesia boundary glasses. *J. Am. Ceram. Soc.*, 1990, **73**, 3677–3683.
33. Powell-Dogan, C. A., Heuer, A. H., Ready, M. J. and Merriam, K., Residual stress-induced grain pullout in a 96% alumina ceramic. *J. Am. Ceram. Soc.*, 1991, **74**, 646–649.
34. Davidge, R. W. and Riley, F. L., Grain-size dependence of the wear of alumina. *Wear*, 1995, 45–49, 186–187.